Developments in the Built Environment 24 (2025) 100772

Contents lists available at ScienceDirect

Developments in the Built Environment

journal homepage: www.sciencedirect.com/journal/developments-in-the-built-environment

Effect of particle shape on mechanical properties of recycled concrete particles under the critical state soil mechanics

Hao Yang [a,b,c], Huishan Wen [a,b,c], Junhui Zhang [a,b,c,*], Fujie Zhao [a,b,c], Ke Liu [a,b,c], Ting Yao [a,d], Mengmeng Wu [e]

[a] Key Laboratory of Special Environment Road Engineering of Hunan Province, Changsha University of Science & Technology, Changsha, Hunan, China
[b] Key Laboratory of Highway Engineering of Ministry of Education, Changsha University of Science & Technology, Changsha, Hunan, China
[c] School of Transportation, Changsha University of Science & Technology, Changsha, Hunan, China
[d] State Key Laboratory of Geomechanics and Geotechnical Engineering, Institute of Rock and Soil Mechanics, Chinese Academy of Sciences, Wuhan, China
[e] Department of Civil and Environmental Engineering, The Hong Kong Polytechnic University, Hung Hom, Hong Kong Special Administrative Region of China

ARTICLE INFO

Keywords:
Particle shape
Construction and demolition wastes
Mechanical properties
Critical state
Discrete element method

ABSTRACT

Recycled concrete particles, a primary component of construction and demolition waste (CDW), significantly contributes to the shear strength of CDW. The influence of particle shape on the mechanical properties of recycled concrete is of importance. This paper constructs four numerical simulation models with varying degrees of sphericity using discrete element simulation. The critical state line (CSL) of the samples is determined through triaxial shearing simulation tests, in conjunction with critical state soil mechanics analysis. The results indicate that particle sphericity markedly affects the macroscopic mechanical properties of recycled concrete particles. With the increase in particle sphericity under higher confining pressure, the deviatoric stress is decreased. Additionally, the cohesion of the samples rises with increasing sphericity, whereas the friction angle decreases. It is worth noting that with the increase of sphericity, the CSL slope of the sample shows a downward trend on both the *q-p'* and *e-log p'* planes.

1. Introduction

Concrete is the most used construction material globally, with its production causing significant environmental impacts, including natural resource depletion and carbon emissions. In response to these challenges, a viable remedy to this challenge lies in the utilization of recycled concrete aggregates (RCA) sourced from construction and demolition waste (CDW) in concrete production (Alibeigibeni et al., 2025; Stochino et al., 2024). Moreover, it has been demonstrated in previous studies that CDW is regarded as an excellent roadbed filling material (Zhang et al., 2019a), and possesses the advantages of favorable compaction performance, high shear strength, strong load-bearing capacity, and good permeability. As a key product for the reduction and high-value utilization of CDW, the mechanical properties of concrete are crucially influenced by the particle morphology of recycled concrete aggregates. Therefore, significant environmental and economic implications are held by the application research of recycled concrete in this context (Ossa et al., 2016; Huang et al., 2025; Huang et al., 2022).

It is worth noting that for the more objective and accurate evaluation of particle morphological characteristics, the morphological indicators of particles have been quantified by scholars using computational geometry. This has enabled the quantitative assessment of particle morphology and provided an important basis for the morphological evaluation of recycled concrete particles. Schwarcz and Shane (1969) first proposed in 1969 that the polar diameter of the particle profile could be expanded using Fourier series to characterize particle morphology. Zhou and Wang (2017) reconstructed the three-dimensional morphology of natural sand particles through spherical harmonic analysis. Owing to the capability of the discrete element method (DEM) to precisely reproduce the complex geometry of particles, and thereby revealing the microscopic mechanism underlying the macroscopic phenomena of materials, the DEM is also widely applied in the research on particle morphology. Dong et al. (2025) classified aggregates based on the flatness index (FI) and elongation index (EI), and the influence laws of aggregate morphological parameters on pore ratio and pore spatial distribution were quantitatively

* Corresponding author. Key Laboratory of Special Environment Road Engineering of Hunan Province, Changsha University of Science & Technology, Changsha, Hunan, China.
E-mail address: zjhseu@csust.edu.cn (J. Zhang).

https://doi.org/10.1016/j.dibe.2025.100772
Received 20 July 2025; Received in revised form 9 September 2025; Accepted 3 October 2025
Available online 3 October 2025

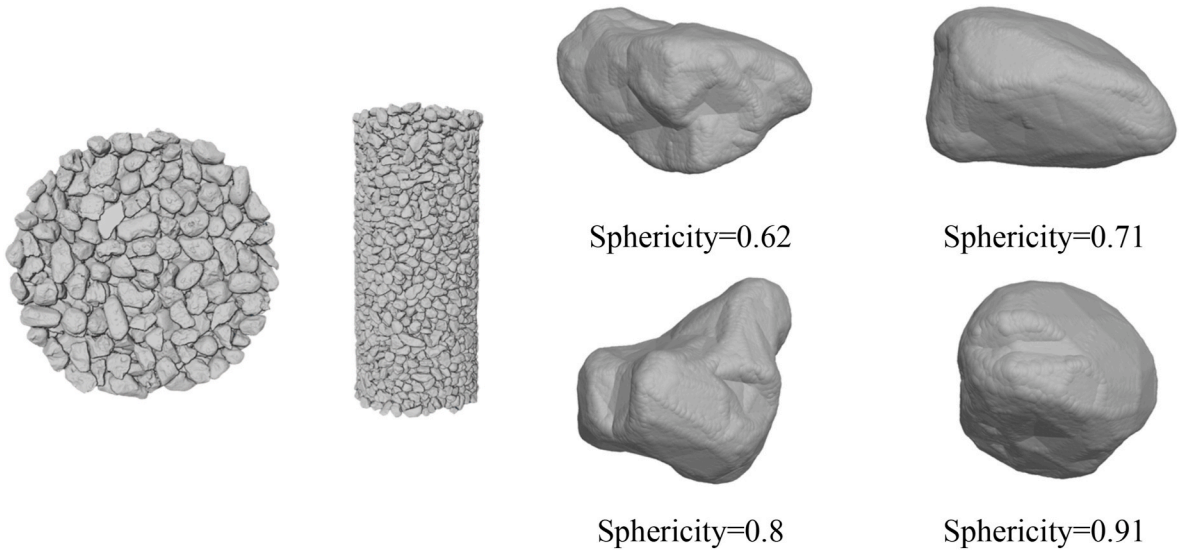

Fig. 1. CT scan images of recycled concrete samples and four three-dimensional extracted images of sphericity.

Table 1
Numerical simulation contact parameters.

Particle-Particle						Particle-Wall		
E(MPa)	kratio	fric	rr_fric	dp_nratio	dp_sratio	E(MPa)	kratio	fric
1.2×10^2	2.3	0.25	0.25	0.5	0.5	1.2×10^2	1.5	0

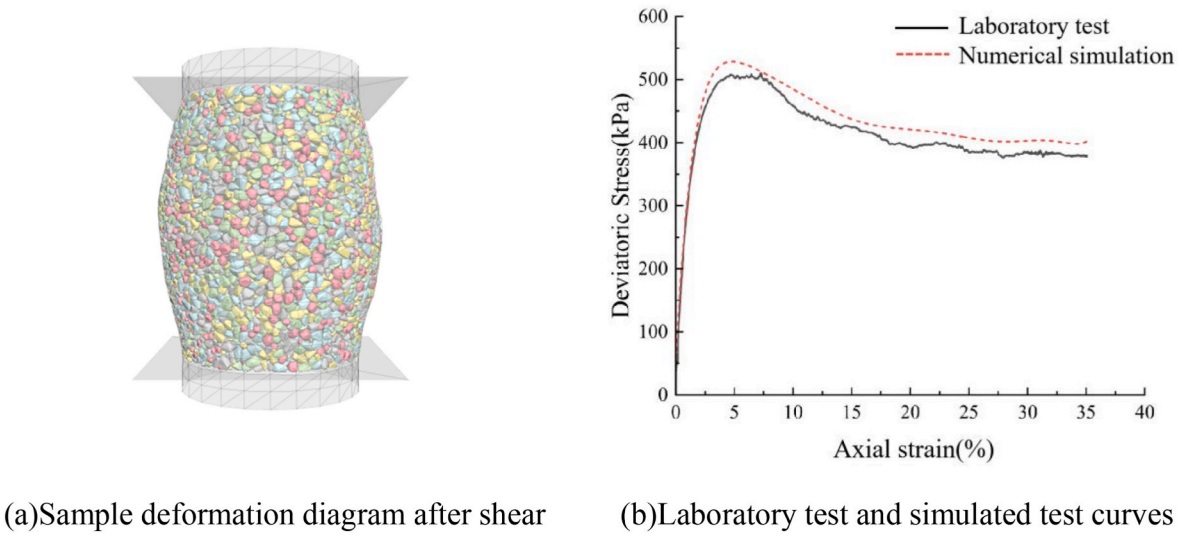

Fig. 2. Particle contact parameter calibration model.

explored through the construction of a discrete element method (DEM) model. Tan et al. (2023) employed DEM to create three stone models by considering different particle shapes and gradations, subsequently performing multiple triaxial compression tests to explore the relationships among these characteristics. The test results revealed that when there is a significant difference in particle characteristics, the angle of the particles is positively correlated with the maximum deviating stress. A high degree of irregularity is generally exhibited in the particle morphology of CDW recycled concrete, which is fundamentally distinct from the particle morphology-focused studies on natural or conventional sand mentioned above. Critical state soil mechanics (CSSM), as a theoretical framework in soil mechanics, is mainly used to describe the behavior of soil under limit states. Therefore, the application of the DEM to the particle shape and combine the critical state soil mechanics analysis to fit the critical state line (CSL) of the sample for recycled concrete aggregates are deemed highly necessary.

2. Background

2.1. Construction and demolition wastes

With the increasing recognition within the engineering field, research on the mechanical response of CDW recycled material has yielded significant results in both field and laboratory tests. Recycled CDW, processed through crushing and screening, is extensively utilized in the production of civil engineering raw materials, including formed

bricks and blocks, asphalt mixtures, recycled aggregates for cement concrete, and alternative materials for pavement engineering (Ossa et al., 2016). Zhang et al. (2019b) conducted and detailed field tests on the construction of highway embankments utilizing CDW recycled material. By employing a light deflection meter to measure the in-situ resilience modulus of the embankments, they demonstrated that CDW exhibits a significantly higher subgrade structural bearing capacity compared to clay.

When treated CDW is utilized as an alternative material for pavement, it is primarily applied to the base or subbase layers. Park (2003) investigated the characteristics and performance of dry and wet CDW recycled aggregates as base and subbase materials for concrete pavements. Arulrajah et al. (2014) concluded that the minimum effective friction angle of compacted CDW aggregate satisfies the necessary requirements for pavement materials. Regarding the prevention of road cracking and rutting, Salimi et al. (2025) developed a novel triple waste geopolymer system for sustainable pavement applications by synergistically combining construction solid waste, WTS (water treatment sludge) and SF (silica fume). Sharma and Hymavathi (2016) proposed that CDW recycled aggregates outperform traditional water-stable or lime-stable base materials. The CDW recycled material, obtained through the crushing and screening of construction solid waste, exhibits characteristics akin to those of a "soil-rock mixture filler" or "residual soil" in terms of coarse and fine particle strength, stiffness variation, and a broad distribution of the grading curve.

2.2. Discrete element method

The physical and mechanical properties of granular materials are intricately linked to their geometric forms. Researchers both domestically and internationally primarily investigate this issue through physical experiments and discrete element numerical simulations. Yang et al. (2019) utilized X-ray micro-computed tomography to examine the relationship between three-dimensional particle shape characteristics and particle size, analyzing the mechanical properties of four distinct types of sand based on aspect ratio and sphericity. Theechalit et al. (2024) initially investigates the mechanical behavior of fresh and used ballast grain assemblies through a combination laboratory experiments discrete element modeling. Zhang et al. (2024) used the Voronoi-based breakable block model based on combined finite-discrete element method to investigate failure mechanism of mine pillars and rock-rock bolt interactions. The discrete element method (DEM) enables an examination of the influence of particle morphology on the physical and mechanical properties of materials from a microscopic perspective. Compared with the existing research on particle morphology, the mechanisms of particle fracture and sliding in recycled concrete aggregates will be gained a deeper understanding.

2.3. Particle shape

Scholars have varying opinions regarding the specific classification of particle shape. Early researchers categorized particle shape into four aspects: single particles, particle combinations, particle aggregations, and particle flow. Zhou et al. (2023) further described particle shape by distinguishing between macroscopic, mesoscopic, and microscopic scales.

For a particle, sphericity can be a good apparent reflection of the regularity of the particle. Sphericity is a measure of the proximity between the three-dimensional shape of a particle and a sphere, which is defined as Equation (1).

$$S_p = \frac{\sqrt[3]{36\pi V_p^2}}{Area_{3d}} \tag{1}$$

where, $Area_{3d}$ is the three-dimensional particle surface area and V_p is the particle volume. The value of sphericity is between 0 and 1, and the closer the sphericity is to 1, the closer the three-dimensional shape of the object is to a sphere, and the sphericity of a perfect sphere is equal to 1.

Therefore, in response to the influence of particle shape on mechanical properties, the use of sphericity for analysis has been adopted by numerous scholars (Fei and Narsilio, 2020a; Fei and Narsilio, 2020b; Zhang et al., 2023; Zhou et al., 2018; Li et al., 2023). However, according to the macroscopic deformation law and mechanical properties of recycled concrete are influenced by the physical and mechanical properties, as well as the shapes of its components, due to the residue of bonded mortar, irregular mechanical damage, and a large number of irregular edges and corners present in recycled concrete particles, the sphericity is not identical to that of natural sand. Additionally, the spatial distribution and characteristics of the contact surfaces between particles play a crucial role. At the microscale, these influences are manifested in the movement and migration of particles within the material. Irregular particle shapes lead to increased obstruction of mutual particle movement, making relative sliding and rotation more challenging. The influence of the shape of recycled concrete particles on the freshness performance of materials has also received extensive attention and research (John Nithin et al., 2025. Mahmoodi et al., 2023; Mahmoodi et al., 2024).

Based on the above background, we classify recycled concrete particles into three levels: (1) Overall shape, (2) Degree of roundness, and (3) Roughness. The overall shape reflects the geometric characteristics of the entire particle, with common indices including fineness length (EI) and flatness (FI). Roundness indicates the sharpness or smoothness of the particle, with common indicators being sphericity and roundness. Roughness describes the degree of local fluctuation on the particle surface, thereby reflecting the texture information of the surface, with roughness being the primary index. The method is employed to characterize the sphericity of particles with circular profiles and quantitatively analyze the influence of sphericity on the macroscopic mechanical properties of recycled concrete.

2.4. Critical state soil mechanics (CSSM)

Critical state soil mechanics (CSSM) is a theoretical framework within soil mechanics, primarily utilized to describe soil behavior at the limit state. CSSM posits that when soil continues to deform along a specific stress path, and both the volume and stress state stabilize, the soil reaches what is referred to as the "critical state". At this critical state, while the strain of the soil may continue to accumulate, the stress and volume remain constant. Bai et al. (2024) classified the damage process and stress-strain response of modified recycled concrete aggregates into two stages: distributed damage and local damage, and considered the critical state as the key point for the development from the distributed damage stage to the local damage stage. The critical state line (CSL) is a fundamental concept in CSSM, representing the relationship between the soil's stress state and its volume under critical conditions. This concept aids engineers in better understanding the interplay between soil stress and volume through a simplified mathematical expression.

3. Numerical simulation test

X-ray μCT technology was employed to scan recycled concrete samples. Avizo software was utilized to calculate the sphericity of the particles within these samples. Four distinct sphericity particle types, exhibiting pronounced morphological differences, were extracted (as shown in Fig. 1), and numerical simulation samples were established as particle templates. The discrete element program was used to simulate the actual particle shapes using rigid block units. Four triaxial specimens of varying sphericity were created by importing the particle scan images shown in Fig. 1. The sample dimensions were consistent with those used in laboratory tests, specifically a cylindrical sample with a diameter of 50 mm and a height of 100 mm. The simulated particle sizes ranged from 0.015 mm to 0.06 mm, ensuring a uniform gradation.

Compared with natural aggregates, due to the lack of cementation among recycled concrete particles, combined with the irregularity, varying sphericity, and surface roughness of non-spherical particles, the rotation of these particles under external forces significantly influences the internal structure of the sample, subsequently affecting the mechanical properties of the soil. Consequently, the contact model between particles employs the rolling resistance linear model, which more accurately simulates the relative rotation trends of irregular particles under external pressure and is better suited for real-world conditions. The contact between the particles and the wall is based on a fundamental linear model.

After selecting the contact model, a 3D image of solid waste particles obtained through X-ray μCT scanning was randomly chosen to establish the sample for parameter calibration. In this simulation, the loading plate in the triaxial test is represented by a rigid wall, while the rubber mold is simulated using shell elements in the finite element analysis. The contact parameters were continuously adjusted through a trial-and-error method, leading to the final determination of the contact parameters (as shown in Table 1). Notably, the samples exhibited significant expansion deformation after shearing, and the calibration curve closely aligns with the laboratory test results (as shown in Fig. 2).

4. Numerical simulation test scheme and results

4.1. Triaxial shearing simulation test scheme

Based on the four particles with varying sphericity depicted in Fig. 1, a total of four samples with distinct sphericity levels were established. Triaxial shearing tests were conducted at confining pressures of 50 kPa, 100 kPa, 200 kPa, and 400 kPa for each sample group, resulting in a total of 16 simulation test groups ($4 \times 4 = 16$). Subsequently, the stress-strain curves, volumetric strain curves, and Mohr circles were analyzed and compared. This analysis comprehensively examines the influence of sphericity on the mechanical properties of recycled concrete samples, integrating principles from critical state soil mechanics.

4.2. Test results

(1) Stress-strain curves

The stress-strain relationship of the sample was analyzed. Fig. 3 illustrates the deviatoric stress-strain curve for samples with varying sphericity under different confining pressure conditions. It is evident from Fig. 3 that the peak deviatoric stress for the same sample increases as confining pressure rises. Samples with lower sphericity (Fig. 3(a) and (b)), characterized by more edges and angles, exhibit a pronounced strain hardening in their stress-strain curves. After reaching the peak deviatoric stress, the deviatoric stress gradually flattens with increasing strain, indicating robust shear resistance. In contrast, samples with higher sphericity (Fig. 3(c) and (d)) display a rounder and less angular shape, resulting in a stress-strain curve that demonstrates strain softening. Following the attainment of the peak deviatoric stress, the deviatoric stress decreases with increasing strain. Concurrently, as sphericity decreases, the axial strain increases when the specimen reaches the peak deviatoric stress.

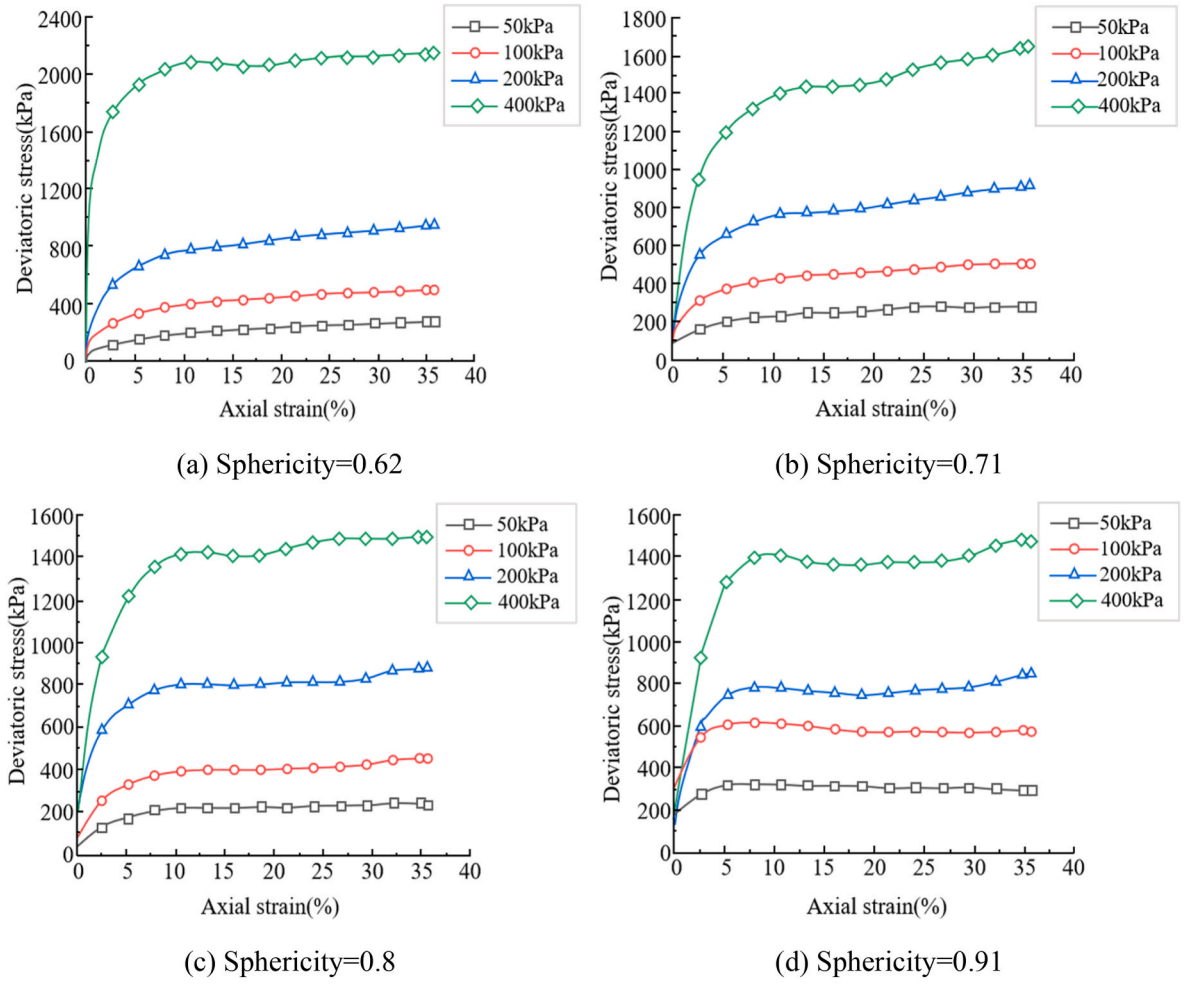

Fig. 3. Stress-strain curves of samples with different particle shapes.

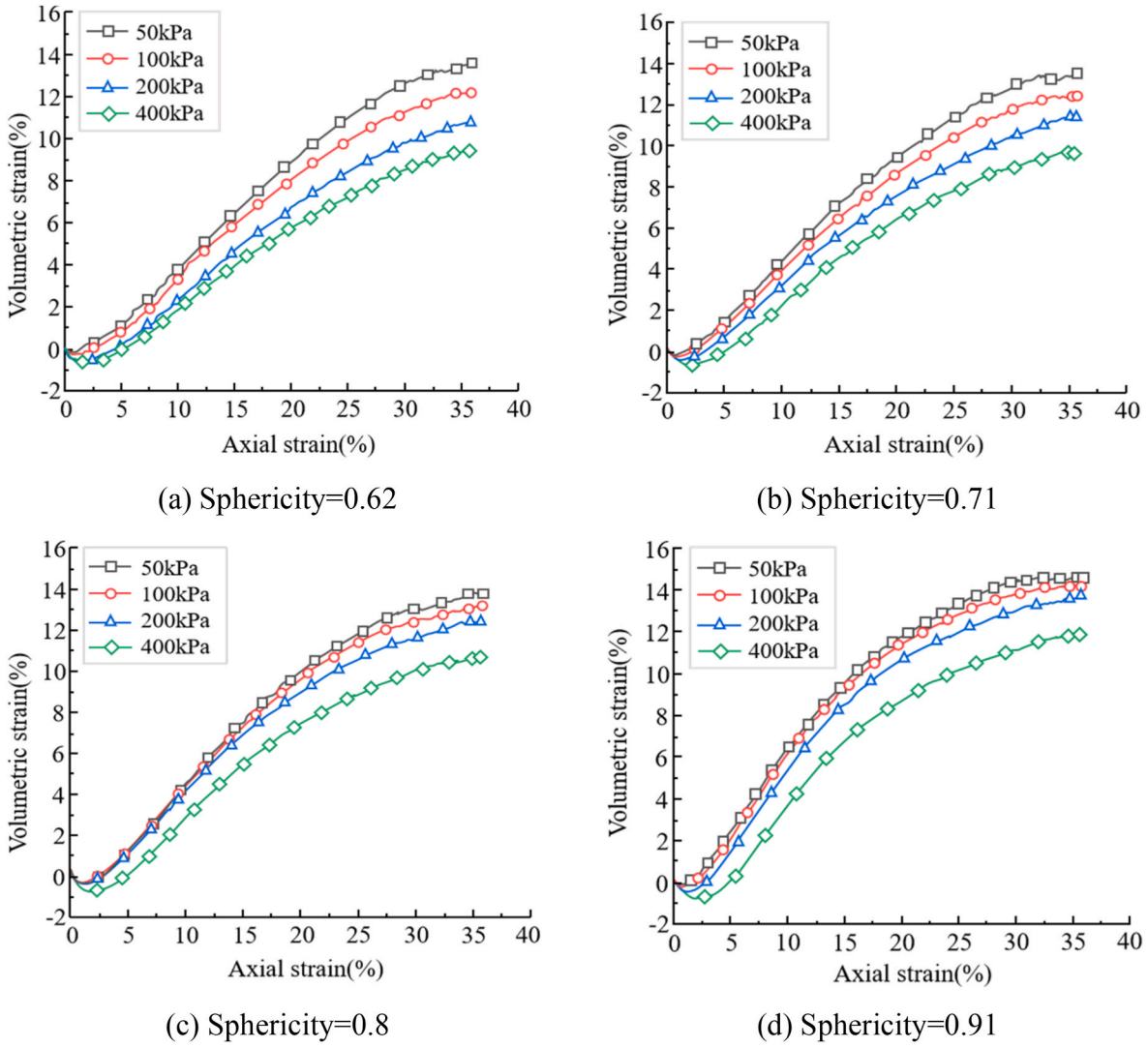

Fig. 4. Volumetric strain curves of samples with different particle shapes.

(2) Volumetric strain curves

The relationship between volumetric strain and axial strain of the sample is illustrated in Fig. 4. As depicted, the volume of all samples initially decreases before subsequently increasing; shear shrinkage occurs first, followed by dilatancy, resulting in a final volume that exceeds that of the sample prior to testing. The axial strain of the specimen gradually increases as sphericity decreases. Additionally, the maximum compression of the specimen's volume increases with rising confining pressure, while the final volume increment of the specimen diminishes as confining pressure increases. All samples exhibited pronounced dilatancy, which decreased with higher confining pressure. This phenomenon can be attributed to the closer arrangement of particles under greater external loads, whereby the increase in pore space between particles is not as significant as that observed under lower confining pressures, leading to a reduced volume change as confining pressure rises.

5. Analysis of test results

5.1. Effect of sphericity on macroscopic mechanical response

To facilitate a more direct comparison of the influence of sphericity on the mechanical properties of samples, we compared the stress-strain curves and volumetric strain curves of samples exhibiting varying degrees of sphericity under identical confining pressure.

Fig. 5 illustrates the deviatoric stress-strain curves for each sample under varying confining pressures. During the initial phase of axial strain, which ranges from 0 % to 5 %, all curves exhibit a consistent trend characterized by a rapid increase in stress, primarily attributed to the elastic deformation of the samples during initial loading. Under low confining pressure conditions (50 kPa and 100 kPa), no obvious correlation exists between the peak deviatoric stress and sphericity. Notably, the peak deviatoric stress is recorded in samples with low sphericity, while the deviatoric stress of particles with high sphericity continues to rise. Conversely, at higher confining pressures (200 kPa and 400 kPa), the deviatoric stress of particles with low sphericity (Sp0.62 and Sp0.71) gradually surpasses that of particles with high sphericity (Sp0.8 and Sp0.91) throughout the shear process, indicating that deviatoric stress increases as sphericity decreases. This phenomenon can be explained by the fact that lower sphericity correlates with coarser, more angular shapes, which enhance interlocking and occlusion effects between particles under external loads. Consequently, achieving the same strain state during loading requires greater external loads, a trend that is particularly pronounced under high confining pressure conditions. Additionally, the irregular shapes of the particles contribute to the specimen's ability to maintain its stress state, resulting in a progressively slower rate of decrease in deviatoric stress. The deviatoric stress-strain

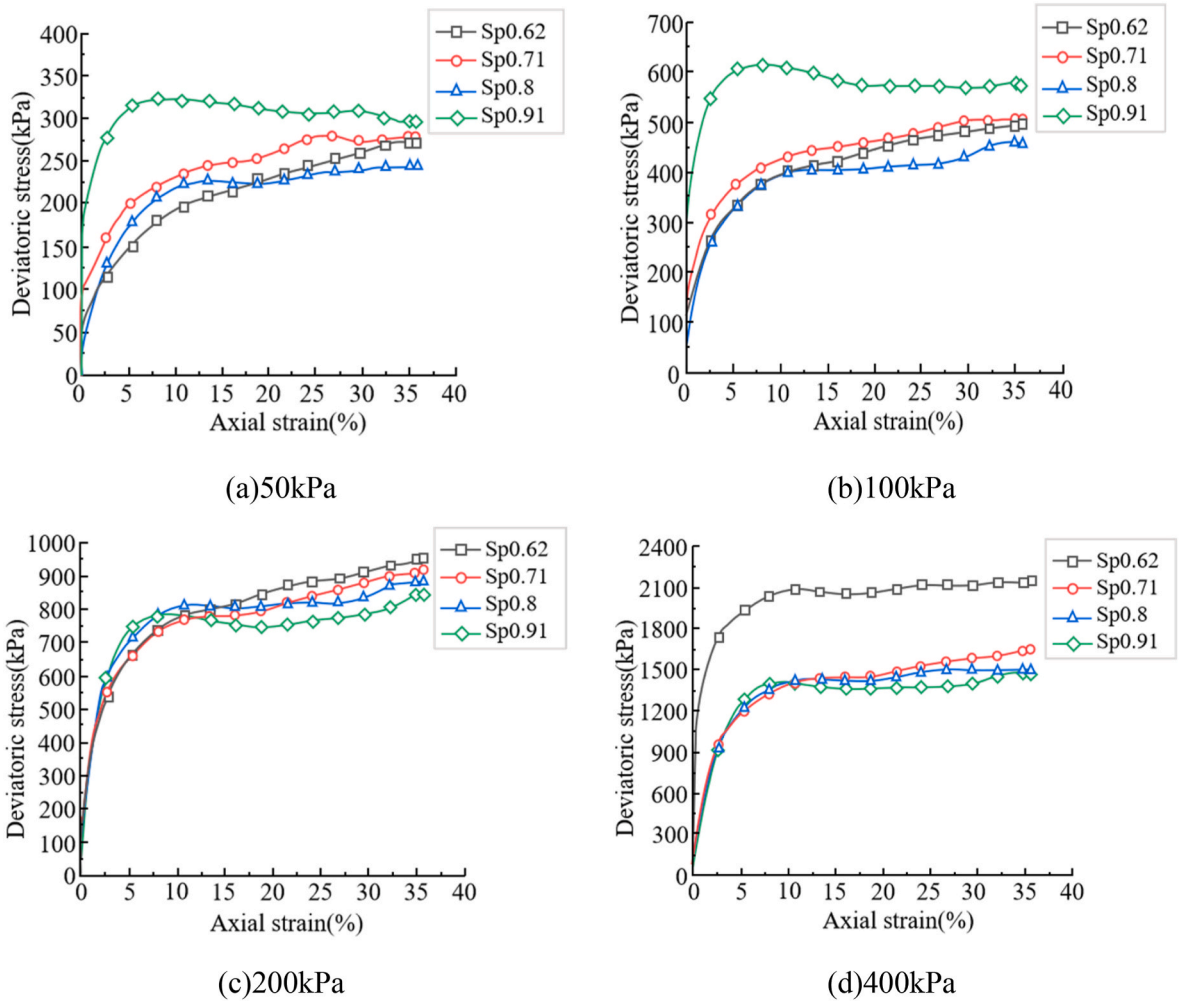

Fig. 5. Stress-strain curves of each sample under different confining pressures.

curve for particles with low sphericity demonstrates a tendency toward strain hardening, whereas particles with high sphericity exhibit a clear tendency toward strain softening.

Generally, sphericity significantly affects the stress-strain characteristics of samples subjected to high confining pressure. Specifically, specimens with low sphericity demonstrate higher shear strength and enhanced stability during shearing, whereas specimens with high sphericity exhibit lower shear strength and a more pronounced softening phenomenon.

Fig. 6 illustrates the volumetric strain curve for each sample under varying confining pressures. Overall, the dilatancy of samples exhibiting higher sphericity occurs earlier, while the maximum shear shrinkage decreases with increasing sphericity. Conversely, the maximum dilatancy rises with greater sphericity, indicating that samples with higher sphericity experience a more pronounced volumetric deformation effect when subjected to external loads.

Within the axial strain range of 0%–5%, the volumetric strain variation trend across all samples is similar, reflecting the initial compression stage. During this stage, the impact of differing sphericity on volumetric strain is relatively minor. As the axial strain increases from 5% to 20%, the volumetric strain curves begin to diverge, with samples of higher sphericity exhibiting more pronounced dilatancy. Beyond an axial strain of 20%, the volumetric strain for all samples stabilizes. As sphericity increases, the volumetric strain during the triaxial shear test demonstrates a more significant shearing trend. In summary, sphericity exerts a considerable influence on the volumetric strain of the samples; higher sphericity correlates with a more substantial volume deformation effect, likely linked to the structural density and internal particle arrangement of the samples.

5.2. *Effect of sphericity on shear strength*

According to the Mohr-Coulomb strength theory, the molar stress circles and shear strength curves of samples with varying sphericity at different confining pressures were plotted to illustrate the peak state of deviatoric stress (as shown in Fig. 7).

The calculated cohesion and friction angles are recorded in Fig. 8 to analyze the influence of sphericity on shear strength. As illustrated in Fig. 8, the cohesion of the sample increases with sphericity, with the most significant increase occurring between Sp0.8 and Sp0.91. This phenomenon can be attributed to the smoother surfaces of particles with higher sphericity, which leads to a relatively smaller contact area.

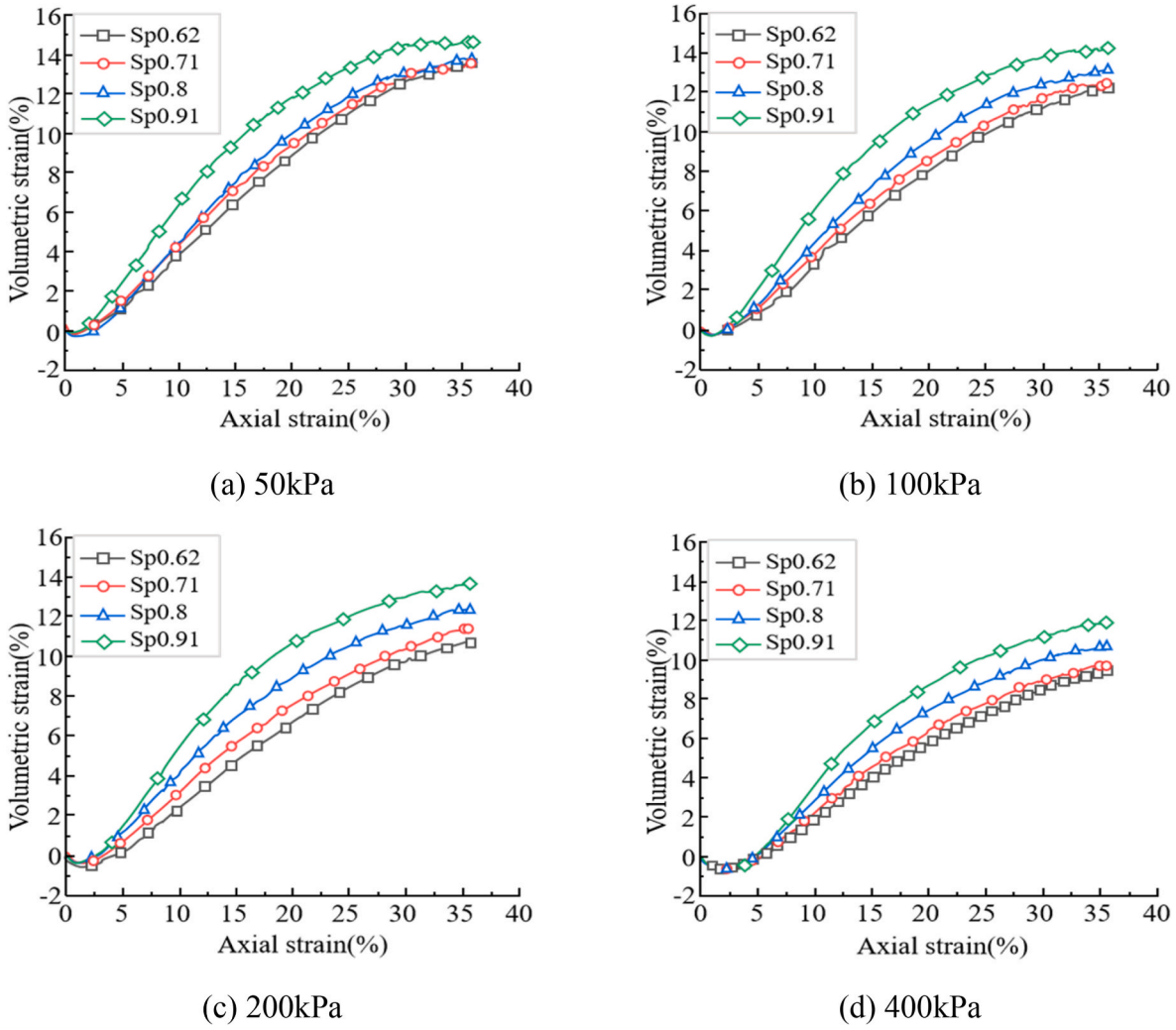

Fig. 6. Volumetric strain curves of each sample under different confining pressures.

Theoretically, this should reduce friction between particles. However, the actual frictional force is influenced not only by the contact area but also by the strength and distribution of the contact points. Increased sphericity facilitates a tighter and more regular arrangement of particles, enhancing the overall stability of the structure. This close arrangement allows for a more even and effective transfer of load and stress, thereby improving the cohesion of the overall structure. In contrast to irregular particles with lower sphericity, this uniform stress distribution minimizes local stress concentrations, further enhancing the material's overall cohesion. Additionally, in the DEM model, the cohesive force between particles is typically simulated to reflect the interactions among them. Due to the regular arrangement and uniformity of contact, spherical particles are more likely to exhibit a uniform distribution of these bonding points, resulting in higher cohesion at the macro level.

The friction angle of the sample decreases as sphericity increases, with a relatively gentle attenuation amplitude observed between different levels of sphericity. This phenomenon occurs because particles with high sphericity closely resemble an ideal spherical shape, allowing them to slide over each other more easily upon contact. Consequently, the interlocking and extrusion forces between these particles are weaker, leading to a reduced frictional resistance. Additionally, particles exhibiting higher sphericity can form a more regular structural arrangement, which enhances the dense packing of particles. In such a dense configuration, vertical pressure among the particles increases; however, the resistance encountered during shearing diminishes due to the smaller contact area and the sliding characteristics at the contact points. This interplay results in a reduction of the friction angle. Furthermore, in granular materials, the formation of force chains is crucial for determining the material's shear strength. The uniform shape and arrangement of spherical particles may lead to shorter or more evenly distributed force chains, thereby decreasing local stress concentrations compared to the longer force chains that can develop in accumulations of non-spherical particles. This aspect also contributes to the observed reduction in the friction angle.

Fig. 9 illustrates the trend of peak deviatoric stress values in relation to sphericity across each group. As sphericity increases, the peak deviatoric stress values in each curve exhibit a decreasing or flattening trend. At confining pressures of 50 kPa, 100 kPa, and 200 kPa, the peak deviatoric stress remains relatively stable or decreases slightly with

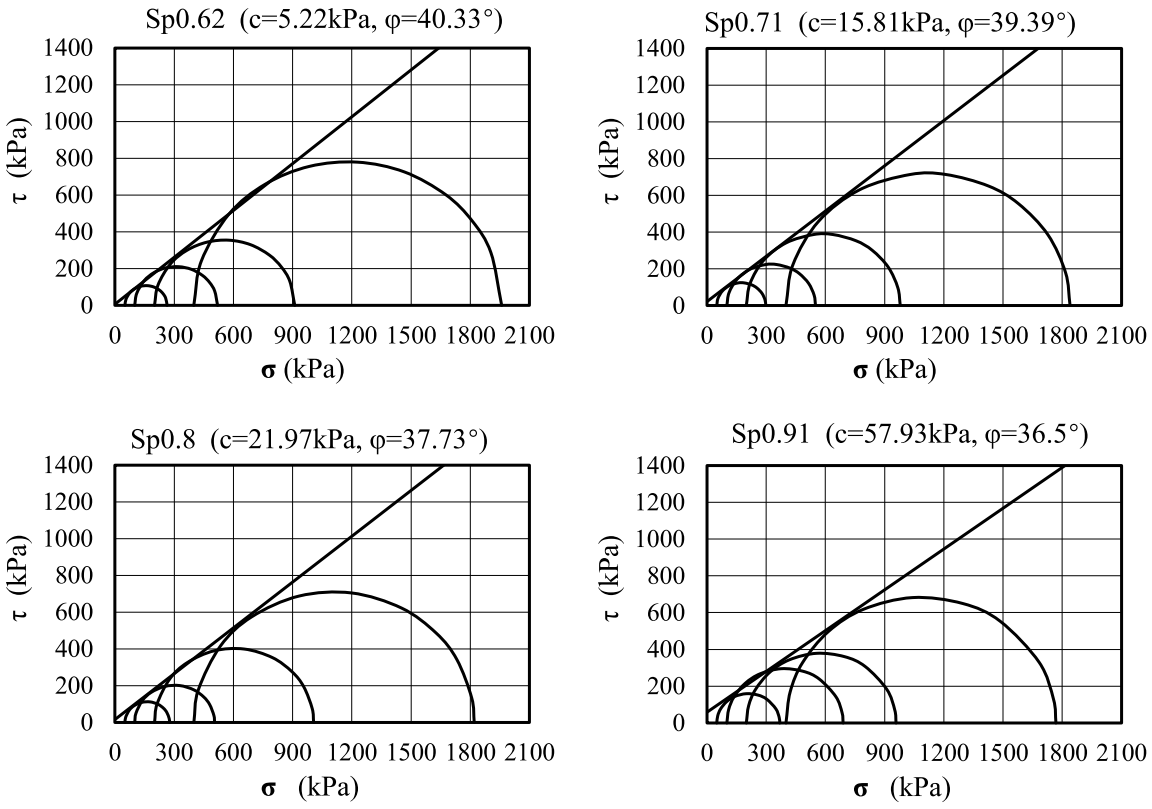

Fig. 7. Shear strength curves of samples with different sphericity.

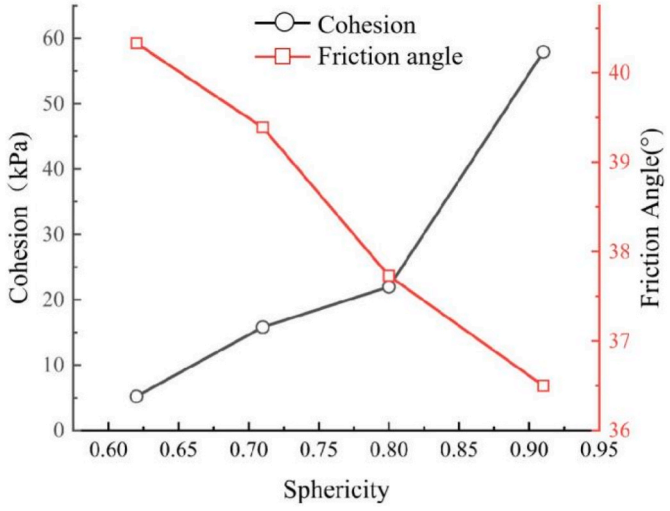

Fig. 8. Relationships between particle sphericity and cohesion, friction angle.

increasing sphericity. However, at a higher confining pressure of 400 kPa, a significant decrease in peak deviatoric stress is observed as sphericity increases, particularly within the range of 0.62–0.8. This indicates that the impact of sphericity on the strength of recycled concrete is more pronounced under high confining pressure conditions. Furthermore, it is evident that greater confining pressure correlates with a higher peak deviatoric stress, consistent with the principle that materials exhibit increased strength under elevated confining pressures.

5.3. Critical state soil mechanics analysis

(1) Critical state line in the *q-p'* plane

As shown in Fig. 10, the critical state point (CSP) of each stress path under confining pressure was found by drawing the *q-p'* curve of each sample, and the CSL was fitted accordingly. In the *q-p'* plane, CSL is usually plotted as a line represented by Equation (2).

$$q_{cs} = M_{cs} p'_{cs} \tag{2}$$

where, the q_{cs} and p'_{cs} are respectively under the critical state of deviatoric stress and the average effective stress, M_{cs} is slope of CSL. There is the following relationship between M_{cs} and the critical state friction Angle Φ_{cs}, as shown in Equation (3).

$$M_{cs} = \frac{q_{cs}}{p_{cs}} = \frac{6\ sin\ \Phi_{cs}}{3 - sin\ \Phi_{cs}} \tag{3}$$

Table 2 and Fig. 10 illustrate that the R^2 values for each fitting curve exceed 0.99, indicating a strong fitting effect. It can be seen from Fig. 11. The slope of the CSL decreases as sphericity increases. Notably, the most significant decline occurs when sphericity increases from 0.62 to 0.71, while the intercept on the longitudinal axis rises with increasing sphericity.

The critical state curve further demonstrates that as sphericity increases, the peak stress that the sample can achieve also decreases, corroborating the previous conclusion. According to critical state theory, once the soil reaches the critical state, its volume, stress state, and shear stress will remain unchanged.

(2) Critical state line in the *e-log p'* plane

The classical representation of CSL in the *e-log p'* plane is a straight line as expressed by Equation (4) (Gajo et al., 2004).

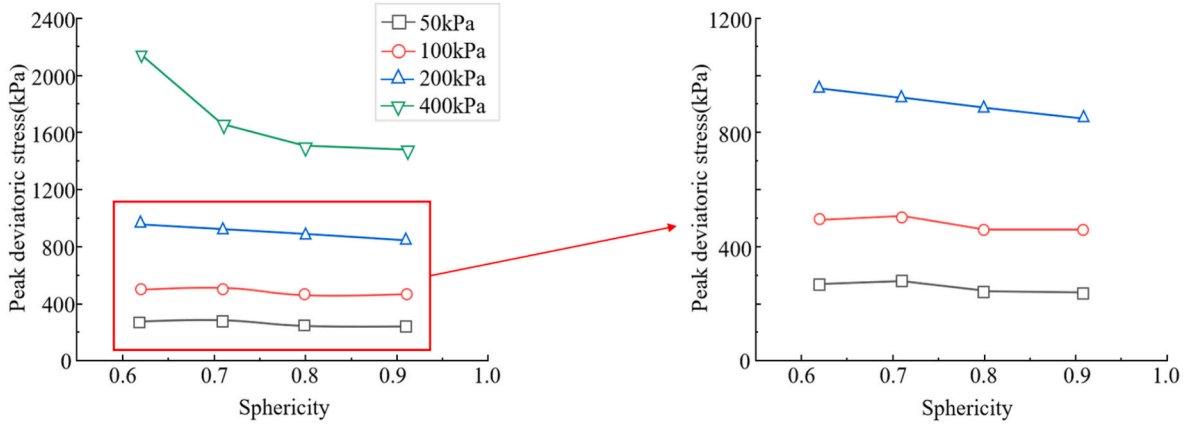

Fig. 9. Relationships between particle sphericity and peak deviatoric stress.

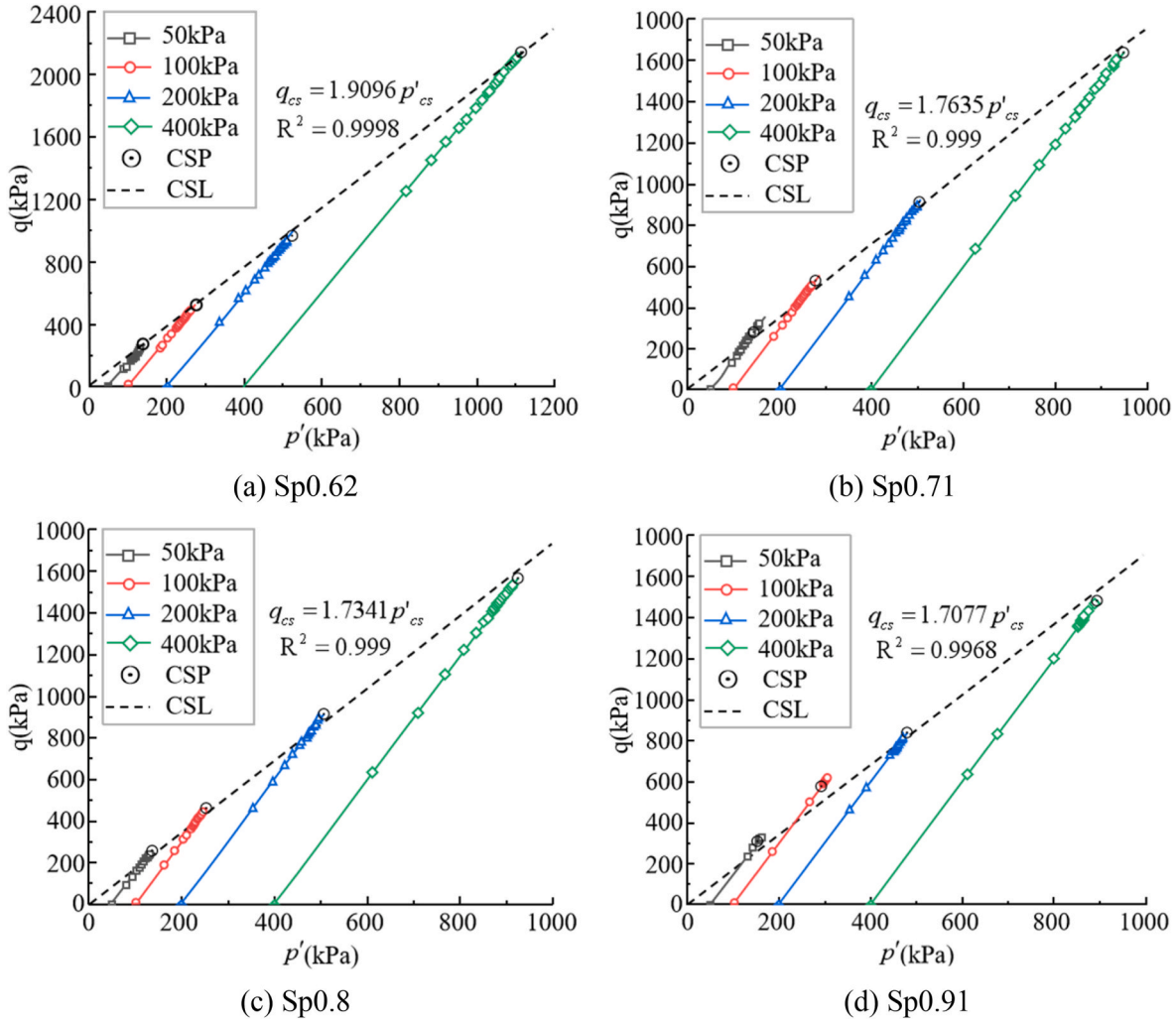

Fig. 10. CSL of samples with different sphericity in *q-p'* plane.

Table 2
The CSL equation of each sample in the *q-p'* plane.

Sample	Slope of CSL in the *q-p'* plane	R^2
Sp0.62	1.9096	0.9998
Sp0.71	1.7635	0.9990
Sp0.8	1.7341	0.9990
Sp0.91	1.7077	0.9968

$$e_{cs} = \Gamma - \lambda \log\left(\frac{p'_{cs}}{1kPa}\right) \tag{4}$$

where, e_{cs} is the pore ratio under critical condition, Γ is the pore ratio intercept when the average effective stress is zero, and λ is the slope of CSL in the semi-log plane. It has been demonstrated that the critical state line (CSL) exists as a curved form in the *e-log p'*, (Li and Wang et al.)

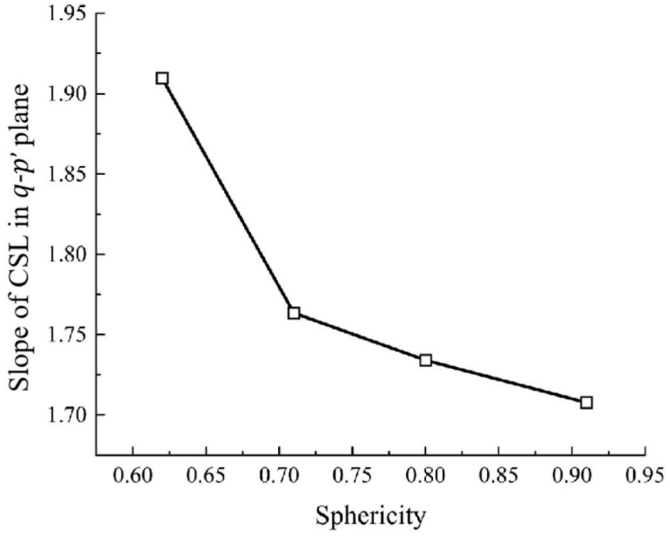

Fig. 11. Sphericity and slope of CSL in the *q-p'* plane.

proposed a power-law model of CSL, as shown in Equation (5).

$$e_{cs} = e_{\Gamma} - \lambda_e \left(\frac{p'_{cs}}{p_a}\right)^a \tag{5}$$

where, p_a is the atmospheric pressure as the reference pressure, e_Γ is the pore ratio intercept, λ_e is the slope of CSL in the power law model, and a is the calibration constant, usually 0.7. Compared with the semi-log model, the power law model can predict the pore ratio intercept of CSL more accurately.

Based in the critical state points extracted from the *e-log p'* curves of each specimen, two forms of the Critical State Line (CSL) were fitted in Figs. 12 and 13, respectively.

Table 3 and Fig. 14 illustrate that as sphericity increases, the slopes of the CSL in the *e-log p'* plane exhibit a distinct downward trend. Additionally, the R^2 values for each fitting curve are consistently above 0.9, indicating a strong fitting effect. The *e-log p'* curves of the samples effectively capture the compression and shear characteristics under varying confining pressure conditions, and the relationship between pore ratio and effective pressure at the critical state is quantitatively described by the fitting equations.

In conclusion, owing to differences in the mechanical properties of various materials, variations are also observed in the slope and intercept

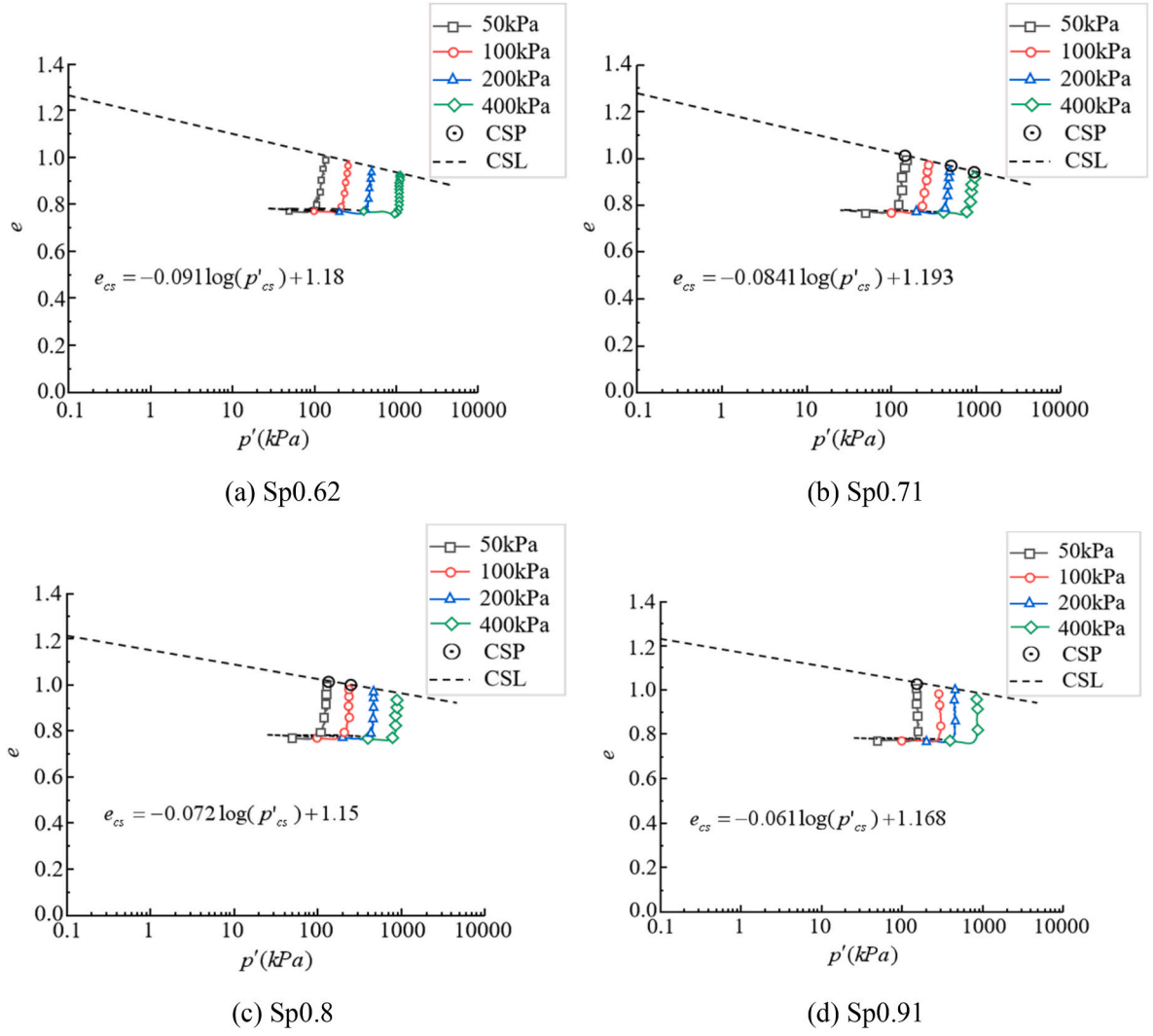

Fig. 12. Semi-log model of CSL in the *e-log p'* plane.

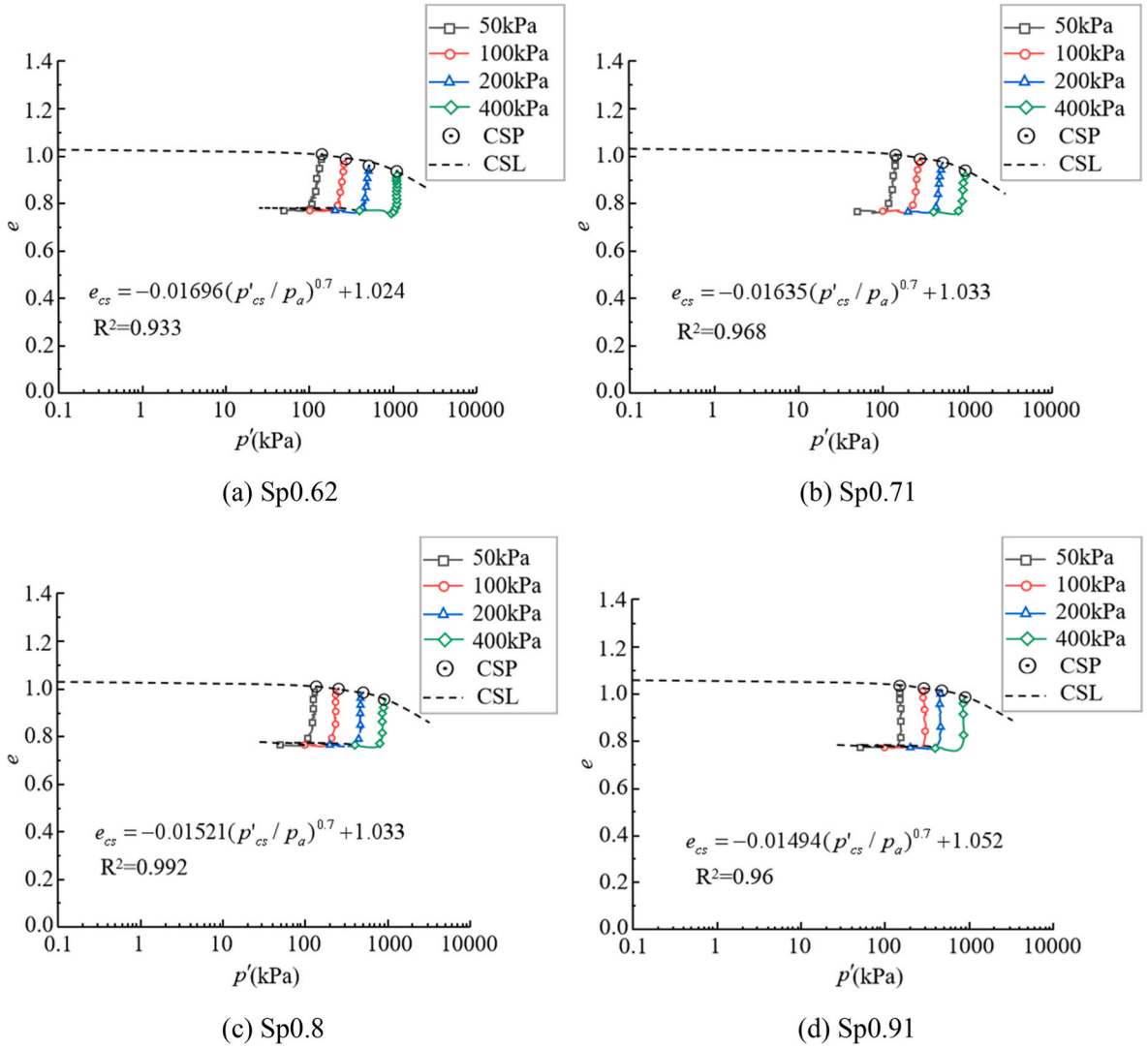

Fig. 13. Power-law model of CSL in the *e-log p'* plane.

Table 3
Comparison of CSL slopes in semi-log and power-law form in *e-log p'* plane.

Sample	Semi-log form	Power-law form
Sp0.62	0.091	0.01696
Sp0.71	0.084	0.01635
Sp0.8	0.072	0.01521
Sp0.91	0.061	0.01494

of the CSL for recycled concrete when compared with those reported (Guo et al., 2024; Yu, 2017; Consoli et al., 2024) in studies on soils, sands, and aggregates.

In addition, the relevant variables affected by its sphericity have been plotted in Fig. 15. The CSL signifies the stable state of soil under limiting conditions. Regardless of the extent of shear deformation experienced by the soil, it will ultimately converge towards this curve, which is crucial for understanding the ultimate bearing capacity and deformation characteristics of the soil. Furthermore, The critical state strength of the soil can be determined from the CSL. This strength

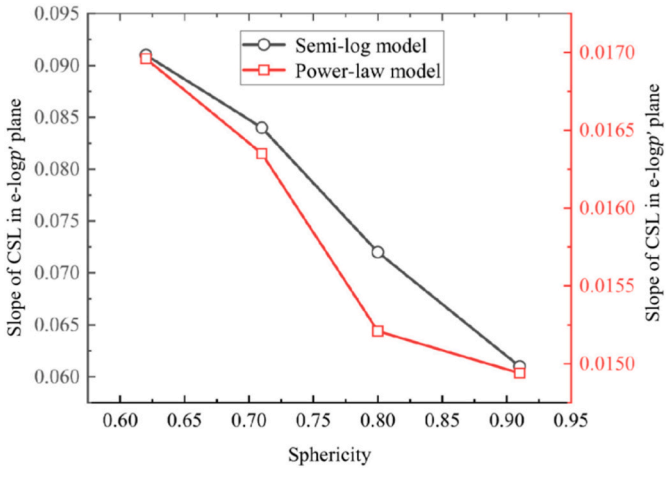

Fig. 14. Sphericity versus CSL slope in the *e*-log *p'* plane.

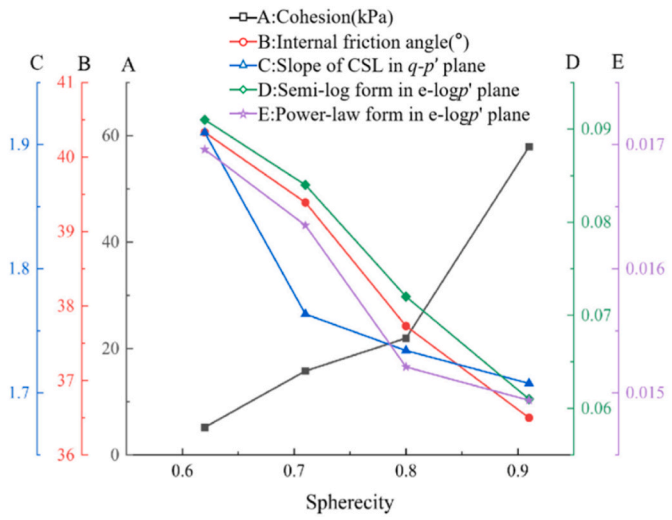

Fig. 15. Relationship between sphericity and each index.

reflects the maximum shear resistance of soil under ultimate conditions, which is vital for stability analysis in engineering design.

6. Conclusion

Four series of numerical simulation tests with varying degrees of particle sphericity were constructed by the DEM. Through triaxial shearing simulation tests, the effect of particle shape on mechanical properties of recycled concrete particles under the CSSM was investigated. Some of the main findings are listed in the following points.

(1) Under the same test conditions, sphericity significantly influences the macroscopic mechanical properties of the sample. As sphericity increases, the stress-strain curve transitions from strain hardening to strain softening. Moreover, specimens exhibiting high sphericity demonstrate lower shear strength and a more pronounced softening phenomenon.
(2) Sphericity significantly impacts the dilatancy characteristics of the specimen. As sphericity increases, the volumetric strain during the triaxial shearing test exhibits a greater dilatancy trend, with the maximum shear shrinkage of the specimen decreasing while the maximum dilatancy increases. Additionally, the sdilatancy in specimens with higher sphericity occurs earlier.
(3) As sphericity increases, the cohesion of the sample gradually rises, with the most significant increase observed between Sp0.8 and Sp0.91. But the friction angle shows a decreasing trend, with a relatively gentle attenuation between different sphericities, while the shear strength of the sample also decreases progressively.
(4) The strength of recycled concrete is significantly influenced by sphericity in high confining pressure environments. The deviatoric stress of the sample gradually decreases with increasing sphericity and shear. The influence of sphericity on the peak value of eccentric stress is more significant, and the higher confining pressures correspond to greater peak values of deviatoric stress.
(5) Sphericity also significantly influences the slope of the CSL of the samples. The slope of the CSL in the *q-p'* plane decreases with increasing sphericity. Similarly, the slopes of both forms of CSL in the *e-log p'* plane also decline as sphericity increases.

CRediT authorship contribution statement

Hao Yang: Writing – original draft, Funding acquisition, Conceptualization. **Huishan Wen:** Writing – review & editing, Software. **Junhui Zhang:** Funding acquisition. **Fujie Zhao:** Formal analysis. **Ke Liu:** Data curation. **Ting Yao:** Investigation. **Mengmeng Wu:** Visualization.

Declaration of competing interest

The authors declare that they have no known competing financial interests or personal relationships that could have appeared to influence the work reported in this paper.

Acknowledgments

This study was funded by the National Science Foundation for Distinguished Young Scholars of China (No. 52025085), the National Natural Science Foundation of China (No. 52208421), the International Cooperation and Exchange of the National Natural Science Foundation of China (No. 52361165623), the National Natural Science Foundation of China (No. 52408394), the Hunan Provincial Natural Science Foundation of China (No. 2023JJ40050), the Science Fund for Creative Research Groups of Hunan Provincial Natural Science Foundation (No. 2024JJ1001), the Open Fund of the Key Laboratory of Special Environment Road Engineering of Hunan Province (Changsha University of Science & Technology) (No. kfj220503).

Data availability

Data will be made available on request.

References

Alibeigibeni, A., Stochino, F., Zucca, M., et al., 2025. Enhancing concrete sustainability: a critical review of the performance of recycled concrete aggregates (RCAs) in structural concrete. Buildings 15 (8), 1361. https://doi.org/10.3390/buildings15081361.

Arulrajah, A., Disfani, M., Horpibulsuk, S., et al., 2014. Physical properties and shear strength responses of recycled construction and demolition materials in unbound pavement base/subbase applications. Constr. Build. Mater. 58, 245–257. https://doi.org/10.1016/j.conbuildmat.2014.02.025.

Bai, W, Geng, Y, Yuan, C, et al., 2024. Study on mechanical properties and mesoscopic damage mechanism of metakaolin modified recycled aggregate concrete. Develop. Built. Environ. 17, 100332. https://doi.org/10.1016/j.dibe.2024.100332.

Consoli, N.C., Azambuja Carvalho, J.V.D., Wagner, A.C., et al., 2024. Determination of critical state line (CSL) for silty-sandy iron ore tailings subjected to low-high confining pressures. J. Rock Mech. Geotech. Eng. 16 (5), 1684–1695. https://doi.org/10.1016/j.jrmge.2023.06.014.

Dong, X, Wu, D, Xiao, X, et al., 2025. A study on the influence of aggregate shape on the aggregate void ratio and stress-strain performance of pervious concrete (PC). Develop. Built. Environ. 23, 100704. https://doi.org/10.1016/j.dibe.2025.100704.

Fei, W., Narsilio, G., 2020a. Impact of three-dimensional sphericity and roundness on coordination number. J. Geotech. Geoenviron. Eng. 146 (12). https://doi.org/10.1061/(asce)gt.1943-5606.0002389, 0-0.

Fei, W., Narsilio, G., 2020b. Impact of three-dimensional sphericity and roundness on coordination number. J. Geotech. Geoenviron. Eng. 146 (12). https://doi.org/10.1061/(asce)gt.1943-5606.0002389, 0-0.

Gajo, A, Bigoni, D, Wood, D, 2004. Multiple shear band development and related instabilities in granular materials. J. Mech. Phys. Solid. 52 (12), 2683–2724.

Guo, W., Song, D., Li, X., 2024. Unified model of critical state line for rockfill material with and without considering particle breakage. Acta Geotechnica 19 (4), 2273–2291. https://doi.org/10.1007/s11440-023-02095-w.

Li X, Wang Y. Linear representation of steady-state line for sand. J. Geotech. Geoenviron. Eng., 124(12), 1215–1217.

Huang, X, Ouyang, Y, Zhang, D, et al., 2025. Greenhouse gas emission of recycled concrete production for pavement construction considering carbon uptake. Develop. Built. Environ. 22, 100646. https://doi.org/10.1016/j.dibe.2025.100646.

Huang, C, Zhang, J, Zhang, A, et al., 2022. Permanent deformation and prediction model of construction and demolition waste under repeated loading. J. Cent. S. Univ.,29 4, 1363–1375. https://doi.org/10.1007/s11771-022-5001-1.

John Nithin, J, Siddhesh, W, Anjan, P., 2025. Effects of particle shape and size on strength and durability of recycled concrete aggregates: an experimental and statistical approach. Constr. Build. Mater. 483, 141718. https://doi.org/10.1016/j.conbuildmat.2025.141718.

Li, J, Zhang, H, Li, Z, et al., 2023. Wetting characteristic and flow behavior of silicate binder at various sand particle-particle interfaces: fine or coarse, circular or angular particles. J. Mater. Res. Technol. 26, 7166–7181. https://doi.org/10.1016/j.jmrt.2023.09.066.

Mahmoodi, O, Siad, H, Lachemi, M, et al., 2023. Effects of Mono and binary recycled aggregates on the rheological properties of geopolymer mortars synthesized with construction and demolition waste-based binders. J. Build. Eng 77, 107545. https://doi.org/10.1016/j.jobe.2023.107545.

Mahmoodi, O, Siad, H, Lachemi, M, et al., 2024. Combined application of CDWs as precursors and aggregates in geopolymer composites: a comprehensive rheological analysis. J. Build. Eng 91, 109574. https://doi.org/10.1016/j.jobe.2024.109574.

Ossa, A., García, J., Botero, E., 2016. Use of recycled construction and demolition waste (CDW) aggregates: a sustainable alternative for the pavement construction industry. J. Clean. Prod. 135, 379–386. https://doi.org/10.1016/j.jclepro.2016.06.088.

Park, T., 2003. Application of construction and building debris as base and subbase materials in rigid pavement. J. Transport. Eng. 129 (5), 558–563. https://doi.org/10.1061/(asce)0733-947x(2003)129:5(558.

Salimi, M, Payan, M, Hosseinpour, I, et al., 2025. Geopolymer stabilization of construction and demolition waste using water treatment sludge and silica fume for pavement applications. J. Mater. Res. Technol. 37, 1834–1849. https://doi.org/10.1016/j.jmrt.2025.06.096.

Schwarcz, H., Shane, K., 1969. Measurement of particle shape by fourier analysis. Sedimentology 13 (3-4), 213–231.

Sharma, R., Hymavathi, J., 2016. Effect of fly ash, construction demolition waste and lime on geotechnical characteristics of a clayey soil: a comparative study. Environ. Earth Sci. 75 (5), 1–11. https://doi.org/10.1007/s12665-015-4796-6.

Stochino, F., Alibeigibeni, A., Zucca, M., et al., 2024. Mechanical behavior of composite slabs with recycled concrete aggregates: a preliminary study. Structures 70, 107838. https://doi.org/10.1016/j.istruc.2024.107838.

Tan, X., Qiu, Z., Yin, X., et al., 2023. Effects of particle shape and packing density on the mechanical performance of recycled aggregates for construction purposes. Buildings 13 (9). https://doi.org/10.3390/buildings13092153, 2153-2153.

Theechalit, B, Sararat, K, Peerapong, J, et al., 2024. Assessment of macro and micro mechanical properties of fresh and deteriorated ballast combining laboratory tests and 2D-discrete element methods. Constr. Build. Mater. 420 (0), 135525. https://doi.org/10.1016/j.conbuildmat.2024.135525, 135525.

Yang, H., Zhou, B., Wang, J., 2019. Exploring the effect of 3D grain shape on the packing and mechanical behaviour of sands. Géotech. Lett. 9 (4), 299–304. https://doi.org/10.1680/jgele.18.00227.

Yu, F.W., 2017. Particle breakage and the critical state of sands. Geotechnique 67 (8), 713–719. https://doi.org/10.1680/jgeot.15.P.250.

Zhang, J., Gu, F., Zhang, Y., 2019a. Use of building-related construction and demolition wastes in highway embankment: laboratory and field evaluations. J. Clean. Prod. 230, 1051–1060. https://doi.org/10.1016/j.jclepro.2019.05.182.

Zhang, J., Gu, F., Zhang, Y., 2019b. Use of building-related construction and demolition wastes in highway embankment: laboratory and field evaluations. J. Clean. Prod. 230, 1051–1060. https://doi.org/10.1016/j.jclepro.2019.05.182.

Zhou, B., Wang, J., 2017. Generation of a realistic 3D sand assembly using x-ray micro-computed tomography and spherical harmonic-based principal component analysis. Int. J. Numer. Anal. Methods GeoMech. 41 (1), 93–109. https://doi.org/10.1002/nag.2548.

Zhou, B., Wang, J., Wang, H., 2018. Three-dimensional sphericity, roundness and fractal dimension of sand particles. Geotechnique 68 (1), 18–30. https://doi.org/10.1680/jgeot.16.p.207.

Zhang, M, Min, Q, Zhao, Q, et al., 2023. Effect of aggregate sphericity on the mechanical properties of ERCC based on highly detailed simulation. J. Mater. Res. Technol. 25, 1406–1420. https://doi.org/10.1016/j.jmrt.2023.06.023.

Zhang, S, Qiu, S, Jiang, Q, et al., 2024. Effect of fully-grouted bolts on the failure behaviors of mine pillars: insights from block-based FDEM modeling. Constr. Build. Mater. 419 (0), 135468. https://doi.org/10.1016/j.conbuildmat.2024.135468, 135468.

Zhou, Z., Li, Z., Zhang, J., et al., 2023. DEM investigation on sandy soil behaviors under the influence of particle shape. Powder Technol. https://doi.org/10.1016/j.powtec.2024.119835.